

Cite this: *Nanoscale Adv.*, 2021, 3, 7002

# Morphology effect of ceria supports on gold nanocluster catalyzed CO oxidation

Zhimin Li,<sup>†ab</sup> Xinyu Zhang,<sup>†a</sup> Quanquan Shi,<sup>Ⓛb</sup> Xia Gong,<sup>a</sup> Hui Xu<sup>\*a</sup> and Gao Li<sup>Ⓛb</sup>

The interfacial perimeter is generally viewed as the catalytically active site for a number of chemical reactions over oxide-supported nanogold catalysts. Here, well-defined CeO<sub>2</sub> nanocubes, nanorods and nanopolyhedra are chosen to accommodate atomically precise clusters (e.g. Au<sub>25</sub>(PET)<sub>18</sub>) to give different Au cluster–CeO<sub>2</sub> interfaces. TEM images show that Au particles of ~1.3 nm are uniformly anchored on the ceria surface after annealing in air at 120 °C, which can rule out the size hierarchy of nanogold in CO oxidation studies. The gold nanoclusters are only immobilized on the CeO<sub>2</sub>(200) facet in Au<sub>25</sub>/CeO<sub>2</sub>-C, while they are selectively loaded on CeO<sub>2</sub>(002) and (111) in the Au<sub>25</sub>/CeO<sub>2</sub>-R and Au<sub>25</sub>/CeO<sub>2</sub>-P catalysts. X-ray photoelectron spectroscopy (XPS) and *in situ* infrared CO adsorption experiments clearly demonstrate that the gold species in the Au<sub>25</sub>/CeO<sub>2</sub> samples are similar and partially charged (Au<sup>δ+</sup>, where 0 < δ < 1). It is observed that the catalytic activity decreases in the order of Au/CeO<sub>2</sub>-R ≈ Au/CeO<sub>2</sub>-P > Au/CeO<sub>2</sub>-C in the CO oxidation. And the apparent activation energy over Au<sub>25</sub>/CeO<sub>2</sub>-C (60.5 kJ mol<sup>-1</sup>) is calculated to be about two-fold of that over the Au<sub>25</sub>/CeO<sub>2</sub>-R (28.6 kJ mol<sup>-1</sup>) and Au<sub>25</sub>/CeO<sub>2</sub>-P (31.3 kJ mol<sup>-1</sup>) catalysts. It is mainly tailored by the adsorbed [O] species on the ceria surface, namely, Au<sub>25</sub>/CeO<sub>2</sub>(002) and Au<sub>25</sub>/CeO<sub>2</sub>(111) which were more active than the Au<sub>25</sub>/CeO<sub>2</sub>(200) system in the CO oxidation. These insights at the molecular level may provide guidelines for the design of new oxide-supported nanogold catalysts for aerobic oxidations.

Received 10th September 2021  
Accepted 5th October 2021

DOI: 10.1039/d1na00680k

rsc.li/nanoscale-advances

## Introduction

Since the discovery of active nanogold for efficient CO oxidation (CO + 0.5 O<sub>2</sub> → CO<sub>2</sub>) by Haruta *et al.* in 1987, it has ignited substantial interest in exploring gold nanoparticles (NPs) as a heterogeneous catalyst for a variety of gas and organic reactions.<sup>1–5</sup> Initially, Au NPs were simply loaded on the surface of metal oxides (e.g., TiO<sub>2</sub>, CeO<sub>2</sub>, Fe<sub>3</sub>O<sub>4</sub>, etc.) *via* deposition–precipitation and co-precipitation methods in a basic system (e.g. pH: 8–10).<sup>6</sup> The preferential conversion of trace CO (typically containing <1 v% CO with >99 v% H<sub>2</sub>) is a highly desirable technique for the CO removal in the industrial hydrogen production under mild conditions. It can reduce H<sub>2</sub> consumption and energy loss, as well as prevent the poisoning of the Pt catalyst by CO in the fuel cell.<sup>7</sup>

Although CO oxidation, as a probe reaction to examine the activity for nanogold catalysts, has been widely investigated for over thirty years, the catalytic mechanism is indeed complicated and has not been fully elucidated yet. The valence state of surface Au atoms, the size of Au particles, and the nature of the

support oxide as well as the interaction between Au NPs and the support, can intensely affect the activity of CO oxidation.<sup>8</sup> Usually, carbon monoxide and dioxygen are deemed to be adsorbed and activated on the surface of naked gold NPs and lattice oxygen of reducible oxides in the Mars–van Krevelen mechanism, respectively.<sup>9</sup> And then the activated CO and [O] species move toward each other and react at the perimeter sites of the interface of the oxide-supported nanogold.

Thus, the morphology of the oxides plays an important role in the catalytic processes.<sup>10–13</sup> The gold particles loaded on the nanocrystalline CeO<sub>2</sub> were explored; it is observed that the gold particles on CeO<sub>2</sub>-rods with {100}/{110} facets gave the best performance.<sup>14</sup> Of note, ceria is a reducible oxide, exhibiting unique redox properties and high oxygen storage capacity, and has been widely applied as an excellent support for Au catalysts.<sup>15–18</sup> However, the size of the Au NPs is not uniform on the different shaped ceria supports. The size-hierarchy is also a key factor in the CO oxidation over nanogold catalysts.<sup>8,19</sup> Thus, controlling the well-defined oxide supports and uniform gold NPs is a big challenge in the fundamental research and mechanism study.

Recently, the breakthrough progress of synthesis of atomically precise gold clusters capped by organic ligands (e.g., thiolate) provided a good platform to study the model system (e.g., uniform gold particles) at the molecular or atomic levels.<sup>20,21</sup> These Au clusters have been exploited in gas oxidations (e.g., CO

<sup>a</sup>College of Science, Inner Mongolia Agricultural University, Hohhot 010018, China. E-mail: qqshi@dicp.ac.cn; yqfxxuhui@163.com

<sup>b</sup>State Key Laboratory of Catalysis, Dalian Institute of Chemical Physics, Chinese Academy of Sciences, Dalian 116023, China. E-mail: gaoli@dicp.ac.cn

<sup>†</sup> Z. L. and X. Z. contributed equally to this work.



oxidation) and a series of organic transformation reactions.<sup>22–25</sup> In our previous studies, the capping ligands of the gold clusters (on the surface of ceria) were partially detached under 120 °C annealing (in air), leading to the exposure of gold atoms which interact with the oxide surface.<sup>26</sup> The reactants (*e.g.*, CO) can only be adsorbed and reacted at the perimeter sites of the oxides and nanogold species, as the other surface gold atoms are fully capped with the organic ligands, which can well block off the CO adsorption.

Herein, we introduce a model of the nanogold catalyst: the atomically precise gold clusters (Au<sub>25</sub>(PET)<sub>18</sub>, PET: phenylethanthiolate) are anchored onto the surface of three well-shaped ceria materials (nanorods, nanocubes and nanopolyhedra). The Au<sub>25</sub> clusters are intact after the 120 °C pretreatment to rule out the size hierarchy of nanogold in the CO oxidation tests. An Au<sub>25</sub>/CeO<sub>2</sub>(200) interface is formed in the Au<sub>25</sub>/CeO<sub>2</sub>-C catalyst. And Au<sub>25</sub>/CeO<sub>2</sub>(002) and (111) are found in both Au/CeO<sub>2</sub>-R and Au/CeO<sub>2</sub>-P. The nanogold of Au<sub>25</sub> nanoclusters on the CeO<sub>2</sub> nanorods and nanopolyhedra shows a similar activity and better than that on the CeO<sub>2</sub> nanocubes in the CO oxidation, which is largely associated with the concentration of the [O] species on the ceria surface.

## Experimental

### Immobilization of clusters onto CeO<sub>2</sub>

Well-defined ceria materials with different morphologies (nanocube, nanorod and nanopolyhedra) were prepared according to the reported protocols.<sup>27–29</sup> The Au<sub>25</sub>(PET)<sub>18</sub> clusters are synthesized *via* the reported literature.<sup>30</sup> Typically, 2 g CeO<sub>2</sub> oxide was dispersed in 30 mL ethyl acetate, and then 10 mg Au<sub>25</sub>(PET)<sub>18</sub> cluster (in 10 mL CH<sub>2</sub>Cl<sub>2</sub>) was drop-wise added into the EtOAc solution. After stirring for 2 h, the solids were collected by centrifugation, dried in a vacuum, and treated at 120 °C in air, and were denoted as Au<sub>25</sub>/CeO<sub>2</sub>-C, Au<sub>25</sub>/CeO<sub>2</sub>-R and Au<sub>25</sub>/CeO<sub>2</sub>-P. ICP-MS showed that the gold content of the Au<sub>25</sub>/CeO<sub>2</sub>-C, Au<sub>25</sub>/CeO<sub>2</sub>-R and Au<sub>25</sub>/CeO<sub>2</sub>-P was 0.25%, 0.31%, and 0.23%.

### Catalyst characterization

The specific surface area of the samples was measured on a Micromeritics ASAP 2020 surface area analyzer. Inductively coupled plasma-mass spectrometry (ICP-MS) was performed on a PerkinElmer ICP-MS NexION 300D. TEM and energy dispersive X-ray spectroscopy (EDX) were performed on a Hitachi 7000 transmission electron microscope operated at 75 kV. X-ray photoelectron spectroscopy (XPS) analysis was performed on a VG ESCAB mk-2.

### Catalytic test for CO oxidation

The catalytic activity of these supported nanogold catalysts was evaluated in a fixed bed, continuous flow quartz reactor with gas hourly space velocity (GHSV) ranging from 15 000 mL g<sup>-1</sup> h<sup>-1</sup>. In a typical experiment, 50 mg catalysts were heated to 120 °C at a heating rate of 5 °C min<sup>-1</sup> in an O<sub>2</sub> flow (30 mL min<sup>-1</sup>) and were kept for 2 h to remove the adsorbed species (*e.g.*, CO<sub>2</sub>). And

then the reactor was spontaneously cooled to ambient temperature before switching to the reactant gas mixture consisting of 1 v% CO, 20 v% O<sub>2</sub>, and 79 v% N<sub>2</sub>. The flows of inlet gases were controlled by using mass-flow controllers. The catalyst was conditioned for 0.5 h in this mixture at ambient temperature before the products were analyzed and determined by using an online gas chromatograph and a thermal conductivity detector. Analogous measurements were performed in 20 °C intervals from room temperature to 120 °C. And then, the temperature was dropped to 100 °C and kept for *ca.* 13 h for the durability investigation.

## Results and discussion

### Characterization of Au<sub>25</sub>/CeO<sub>2</sub>

TEM images showed that the Au<sub>25</sub> clusters were loaded on the surface of CeO<sub>2</sub> (Fig. 1). The size of the Au clusters was retained at *ca.* 1.3 nm in all three samples (Au<sub>25</sub>/CeO<sub>2</sub>-C, Au<sub>25</sub>/CeO<sub>2</sub>-R and Au<sub>25</sub>/CeO<sub>2</sub>-P), consistent with our previous studies.<sup>31</sup> Of note, a few protecting thiolate ligands (*ca.* 3–4 thiolate) are detached during the 120 °C annealing process in air, which has been investigated in our previous results.<sup>26</sup>

The size of the nanocube-like CeO<sub>2</sub> oxides is approximately 27.5 ± 12 nm, and only the CeO<sub>2</sub>(200) facet was found in the Au<sub>25</sub>/CeO<sub>2</sub>-C sample, as shown in Fig. 1a and b. And Au<sub>25</sub> clusters were loaded onto the (200) facet. In the case of Au<sub>25</sub>/CeO<sub>2</sub>-P, the oxide particle is *ca.* 10.9 ± 2.7 nm, and two facets of CeO<sub>2</sub>(002) and (111) were observed, which agrees well with the reported results.<sup>27–29</sup> The clusters are attached on both the CeO<sub>2</sub> facets (Fig. 1e and f). With regard to Au<sub>25</sub>/CeO<sub>2</sub>-R, the length and width of the oxides are 50–200 nm and 8–13 nm, and three facets of CeO<sub>2</sub>(002), (111) and (220) are discovered in the TEM analysis. Similar to Au<sub>25</sub>/CeO<sub>2</sub>-P, the Au<sub>25</sub> particles are found to be immobilized on the CeO<sub>2</sub>(002) and (111) facets, as shown in Fig. 1c and d. And we applied EDX analysis to confirm whether the Au<sub>25</sub>(PET)<sub>18</sub> nanoclusters are immobilized onto the ceria surface. As shown in Fig. 2, gold (Au), sulfur (S), oxygen (O), and cerium (Ce) elements are observed in the Au<sub>25</sub>/CeO<sub>2</sub> catalysts, suggesting that the Au<sub>25</sub> clusters should be intact after wet-deposition onto the CeO<sub>2</sub> support.

Further, these as-prepared Au<sub>25</sub>/CeO<sub>2</sub> samples were evaluated by the BET analyses and powder X-ray diffraction (XRD). Five prominent diffraction lines at 28.7, 33.3, 47.8, 56.8 and 59.6° were found in the XRD patterns of all the Au<sub>25</sub>/CeO<sub>2</sub>-P, Au<sub>25</sub>/CeO<sub>2</sub>-R, and Au<sub>25</sub>/CeO<sub>2</sub>-C samples (Fig. 3a), which were assigned to the CeO<sub>2</sub> facets of (111), (200), (220), (311) and (222) (PDF #34-0394). It implied that these nanocube-, nanorod- and nanopolyhedra-like ceria materials exhibited the same phase composition. No diffraction is found for the gold clusters, which is mainly due to the small-sized particles and the low gold loading concentration (Au: 0.23–0.31 wt%). Next, Fig. 3b shows that the BET value for Au<sub>25</sub>/CeO<sub>2</sub>-R, Au<sub>25</sub>/CeO<sub>2</sub>-P and Au<sub>25</sub>/CeO<sub>2</sub>-C is 86.0, 72.5 and 36.2 m<sup>2</sup> g<sup>-1</sup>, respectively. Au<sub>25</sub>/CeO<sub>2</sub>-R and Au<sub>25</sub>/CeO<sub>2</sub>-P showed a larger surface area than Au<sub>25</sub>/CeO<sub>2</sub>-C, which is caused by the size of CeO<sub>2</sub> oxides and mainly by the hydroxyl species on ceria (*vide infra*).



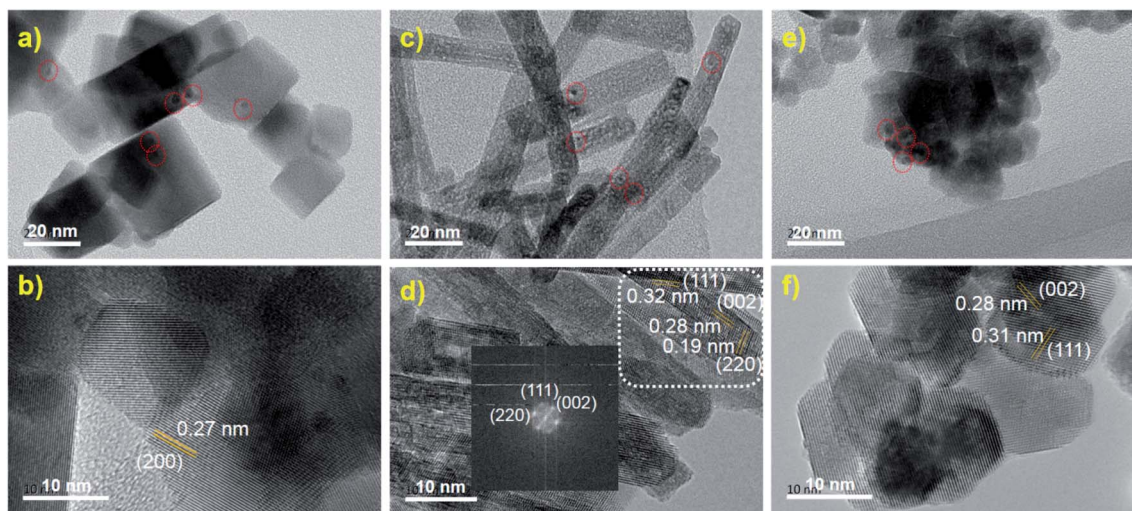


**Fig. 1** TEM images of the (a and b)  $\text{Au}_{25}/\text{CeO}_2\text{-C}$ , (c and d)  $\text{Au}_{25}/\text{CeO}_2\text{-R}$ , and (e and f)  $\text{Au}_{25}/\text{CeO}_2\text{-P}$  catalysts. The gold clusters are highlighted in the red rings, and the particle size is about 1.3 nm, consistent with the size of the unsupported  $\text{Au}_{25}(\text{PET})_{18}$  parent clusters. The inset in (d) is the electron diffraction diagram.

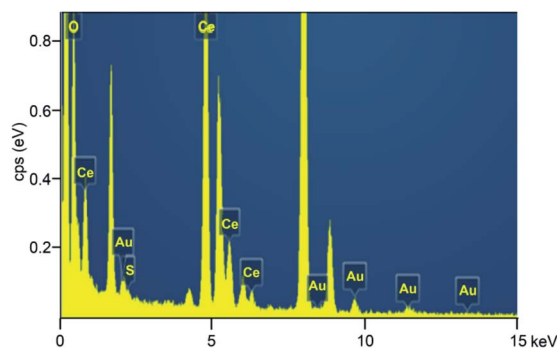


**Fig. 2** EDX analysis of the  $\text{Au}_{25}/\text{CeO}_2$  catalysts.

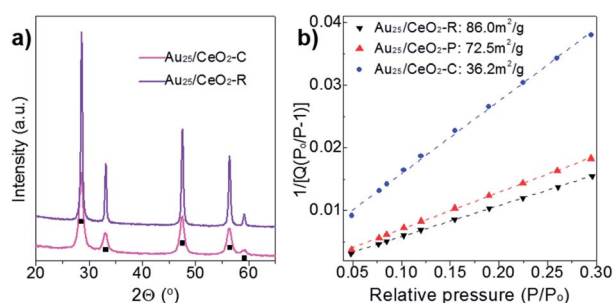


**Fig. 3** (a) XRD patterns and (b) specific surface areas of  $\text{Au}_{25}/\text{CeO}_2\text{-R}$ ,  $\text{Au}_{25}/\text{CeO}_2\text{-P}$  and  $\text{Au}_{25}/\text{CeO}_2\text{-C}$ .

### Catalytic performance in the CO oxidation

These prepared  $\text{CeO}_2$ -supported Au cluster catalysts were evaluated in the CO oxidation in the presence of 1 v% CO and 20 v%  $\text{O}_2$ , as shown in Fig. 4. Interestingly, the  $\text{Au}_{25}/\text{CeO}_2\text{-C}$  catalyst was inert from r.t. to 60 °C and started to give very low CO conversion at 80 °C (8.4%) and 120 °C (64%). In contrast,  $\text{Au}_{25}/$

$\text{CeO}_2\text{-P}$  and  $\text{Au}_{25}/\text{CeO}_2\text{-R}$  showed a similar catalytic activity (Fig. 4a, black and red lines), which is much better than that of  $\text{Au}_{25}/\text{CeO}_2\text{-C}$ . Of note, both  $\text{Au}_{25}/\text{CeO}_2\text{-P}$  and  $\text{Au}_{25}/\text{CeO}_2\text{-R}$  show some activity ( $\sim 3.8\%$  CO conversion) even at room temperature. Hence, the conversion rate is in the order of  $\text{Au}_{25}/\text{CeO}_2\text{-R} \approx \text{Au}_{25}/\text{CeO}_2\text{-P} > \text{Au}_{25}/\text{CeO}_2\text{-C}$ , based on the CO conversion, which is different from the reported results over the naked Au NP system in the water-gas shift reactions (the rate follows the order of  $\text{Au}/\text{CeO}_2\text{-R} > \text{Au}/\text{CeO}_2\text{-P} > \text{Au}_{25}/\text{CeO}_2\text{-C}$ ).<sup>32</sup> It may be because the surface of  $\text{Au}_{25}$  clusters is capped by the thiolate ligands, except the interfacial perimeter sites. Of note, the plain  $\text{CeO}_2$  can only show activity at higher temperature ( $>200$  °C), and its activity is negligible (almost zero conversion of CO) in the present temperature range of r.t. to 120 °C. Notably,  $\text{Au}_{25}/\text{CeO}_2\text{-R}$  showed good durability at 100 °C over 13 h (Fig. 4c). The rate of conversion converged to  $\sim 95\%$  with no appreciable loss of activity, implying that  $\text{Au}_{25}/\text{CeO}_2\text{-R}$  is robust and promising for prolonged periods of time. It should be noted that the  $\text{Au}_{25}$  nanoclusters supported on the ceria surface should be intact under such mild reaction conditions ( $\leq 120$  °C).<sup>26</sup>

Further, the apparent activation energies were calculated and determined to be 28.6, 31.3 and 60.5  $\text{kJ mol}^{-1}$  over  $\text{Au}_{25}/\text{CeO}_2\text{-R}$ ,  $\text{Au}_{25}/\text{CeO}_2\text{-P}$  and  $\text{Au}_{25}/\text{CeO}_2\text{-C}$ , respectively (Fig. 4b). The activation energy over  $\text{Au}_{25}/\text{CeO}_2\text{-C}$  is two fold that of  $\text{Au}_{25}/\text{CeO}_2\text{-R}$  and  $\text{Au}_{25}/\text{CeO}_2\text{-P}$ . It is well known that the CO and dioxygen molecules are activated over the gold particles and ceria surface respectively in the CO oxidation catalyzed by Au/ $\text{CeO}_2$ . And in our previous studies, the CO oxidation over the ceria-supported gold clusters (capped with thiolates) occurred at the perimeter interface between Au particles and the supports, as the surface of gold clusters are well protected by the remaining organic ligands after thermal annealing. Therefore, the chemical state of gold atoms and the lattice facet of ceria play pivotal roles in the CO oxidation over the Au/ $\text{CeO}_2$  system.



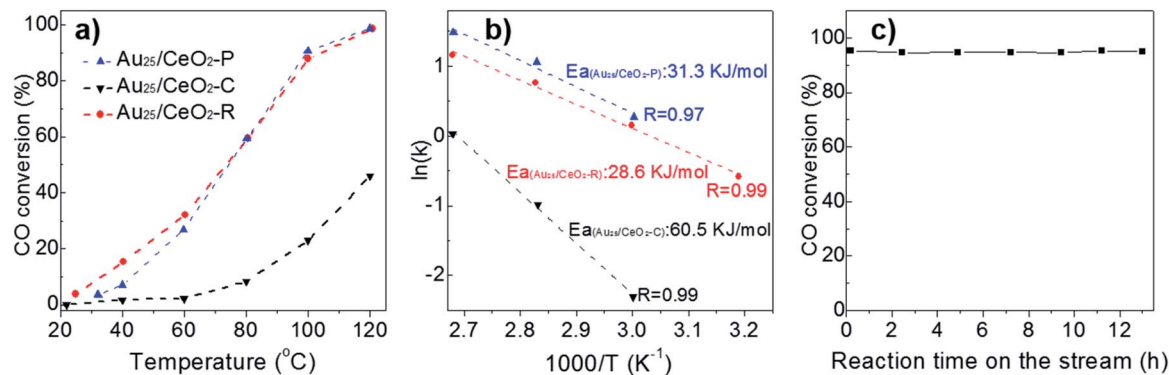


Fig. 4 (a) Catalytic performance of  $\text{Au}_{25}/\text{CeO}_2$  in the CO oxidation. (b) The apparent activation energies over the  $\text{Au}_{25}/\text{CeO}_2\text{-R}$ ,  $\text{Au}_{25}/\text{CeO}_2\text{-P}$  and  $\text{Au}_{25}/\text{CeO}_2\text{-C}$ . (c) The durability of the  $\text{Au}_{25}/\text{CeO}_2\text{-R}$  catalyst at  $100\text{ }^\circ\text{C}$  for  $\sim 13$  h. Reaction conditions: 50 mg catalyst, reactant gas mixture consisting of 1 v% CO, 20 v%  $\text{O}_2$ , and 79 v%  $\text{N}_2$  with a  $15\ 000\ \text{mL g}^{-1}\ \text{h}^{-1}$  GHSV.

### XPS and CO-IR profiles

Therefore, the chemical states of the gold, cerium, and oxygen species were examined by XPS analysis. As shown in Fig. 5a, the binding energies (BEs) of Ce 3d are almost superimposable, indicating that the cerium species is  $\text{Ce}^{4+}$ . With regard to the Au species, all the  $\text{Au}_{25}/\text{CeO}_2\text{-R}$ ,  $\text{Au}_{25}/\text{CeO}_2\text{-P}$  and  $\text{Au}_{25}/\text{CeO}_2\text{-C}$  samples gave the BEs at 87.1 (Au  $4f_{5/2}$ ) and 83.5 eV (Au  $4f_{7/2}$ ) as shown in Fig. 5b, indicating that the chemical states of gold species were the same as  $\text{Au}^{\delta+}$  (where,  $0 < \delta < 1$ ).<sup>33</sup> Moving to the oxygen species on the surface of ceria, two sets of BE peaks are found as shown in Fig. 5c, which are assigned to adsorbed oxygen species ( $\text{O}_A$ , O 1s BE at 531.2 eV) and lattice oxygen ( $\text{O}_L$ , 528.7 eV).<sup>34</sup> After detailed calculations, the ratio of the  $\text{O}_A$  species to  $\text{O}_L$  is decreased as follows:  $\text{Au}_{25}/\text{CeO}_2\text{-R}$  (1.28) >  $\text{Au}_{25}/\text{CeO}_2\text{-P}$  (0.60) >  $\text{Au}_{25}/\text{CeO}_2\text{-C}$  (0.30). Therefore, both the BET and XPS analyses showed that  $\text{Au}_{25}/\text{CeO}_2\text{-R}$  and  $\text{Au}_{25}/\text{CeO}_2\text{-P}$  exhibited more hydroxyl species than the  $\text{Au}_{25}/\text{CeO}_2\text{-C}$  catalyst.

$\text{Au}_{25}/\text{CeO}_2$  samples were investigated by *in situ* infrared CO adsorption experiments at a low temperature of  $-150\text{ }^\circ\text{C}$  (liquid

nitrogen), as shown in Fig. 5d. These samples were pretreated with He flow, and then they were introduced into a CO atmosphere for 5 min. The samples were finally treated with He flow to remove the excess CO. A set of intense bands at  $2142\ \text{cm}^{-1}$  was seen in all  $\text{Au}_{25}/\text{CeO}_2\text{-R}$ ,  $\text{Au}_{25}/\text{CeO}_2\text{-P}$  and  $\text{Au}_{25}/\text{CeO}_2\text{-C}$  samples, which can be attributed to CO adsorbed on the  $\text{Au}^{\delta+}$  species ( $0 < \delta < 1$ ), as the value is between the bands of  $\text{CO-Au}^0$  ( $\sim 2115\ \text{cm}^{-1}$ ) and the  $\text{CO-Au}^+$  ( $\sim 2161\ \text{cm}^{-1}$ ).<sup>35,36</sup> These results matched well with the XPS analyses. Therefore, based on the results of the CO adsorption *operando*-DRIFTS characterization, gold active sites should be associated with the partially oxidized  $\text{Au}^{\delta+}$  ( $0 < \delta < 1$ ) species.

### Conclusions

In conclusion, well-defined  $\text{CeO}_2$  nanocubes (exposing  $\text{CeO}_2(200)$  facet) and nanorods and nanopolyhedra ( $\text{CeO}_2(002)$  and (111)) were adapted to anchor the atomically precise  $\text{Au}_{25}(\text{PET})_{18}$  clusters in this study. Au particles were not aggregated during the annealing at  $120\text{ }^\circ\text{C}$  to rule out the size-hierarchy of nanogold in the CO oxidation. The gold species in the  $\text{Au}_{25}/\text{CeO}_2$  system are the same ( $\text{Au}^{\delta+}$ ,  $0 < \delta < 1$ ). It is found that the catalytic activity decreases in the order of  $\text{Au}_{25}/\text{CeO}_2\text{-R} \approx \text{Au}_{25}/\text{CeO}_2\text{-P} > \text{Au}_{25}/\text{CeO}_2\text{-C}$ , and correspondingly the apparent activation energy of  $\text{Au}_{25}/\text{CeO}_2\text{-C}$  is two-fold that of the  $\text{Au}_{25}/\text{CeO}_2\text{-R}$  and  $\text{Au}_{25}/\text{CeO}_2\text{-P}$  catalysts.  $\text{Au}_{25}/\text{CeO}_2\text{-R}$  exhibited excellent durability in the CO oxidation over 13 h. To sum up, the catalytic activity can be drastically tailored by the adsorbed oxygen species on the facet of ceria, which can provide guidelines for the design of new oxide-supported nanogold catalysts for aerobic oxidations.

### Conflicts of interest

There are no conflicts to declare.

### Acknowledgements

We acknowledge the financial support by the National Natural Science Foundation of China (22065029 and 2217020878),

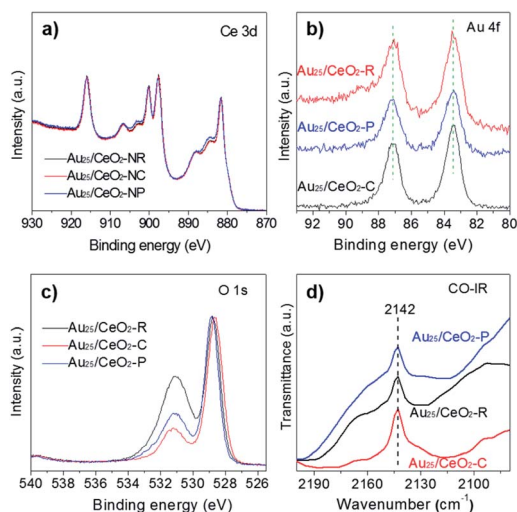


Fig. 5 XPS analysis of the  $\text{Au}_{25}/\text{CeO}_2$  samples: (a) Ce 3d, (b) Au 4f, and (c) O 1s. (d) *Operando*-DRIFTS of CO adsorption on  $\text{Au}_{25}/\text{CeO}_2$  catalysts, which is investigated at  $-150\text{ }^\circ\text{C}$  (liquid nitrogen).



Young Talents of Science and Technology in Universities of Inner Mongolia Autonomous Region (NJYT-20-B20), and Liaoning Natural Science Foundation of China (2020-MS-024).

## Notes and references

- 1 S. Tsubota, D. Cunningham, Y. Bando and M. Haruta, *Stud. Surf. Sci. Catal.*, 1993, **77**, 325–328.
- 2 Z. Li, C. Brouwer and C. He, *Chem. Rev.*, 2008, **108**, 3239–3265.
- 3 A. Corma and H. Garcia, *Chem. Soc. Rev.*, 2008, **37**, 2096–2126.
- 4 G. Li and R. Jin, *Nanotechnol. Rev.*, 2013, **5**, 529–545.
- 5 G. Zhang, R. Wang and G. Li, *Chin. Chem. Lett.*, 2018, **29**, 687–693.
- 6 R. Zanella, S. Giorgio, C. R. Henry and C. Louis, *J. Phys. Chem. B*, 2002, **106**, 7634–7642.
- 7 P. D. Vaidya and A. E. Rodrigues, *Chem. Eng. J.*, 2006, **117**, 39–49.
- 8 A. Taketoshi and M. Haruta, *Chem. Lett.*, 2014, **43**, 380–387.
- 9 D. Widmann and R. J. Behm, *Acc. Chem. Res.*, 2014, **47**, 740–749.
- 10 Y. Li and W. Shen, *Chem. Soc. Rev.*, 2014, **43**, 1543–1574.
- 11 Q. Q. Shi, Y. Li, Y. Zhou, S. Miao, N. Ta, E. S. Zhan, J. Y. Liu and W. J. Shen, *J. Mater. Chem. A*, 2015, **3**, 14409–14415.
- 12 Q. Q. Shi, G. C. Ping, X. J. Wang, H. Xu, J. M. Li, J. Q. Cui, H. Abroshan, H. J. Ding and G. Li, *J. Mater. Chem. A*, 2019, **7**, 2253–2260.
- 13 F. Kollhoff, J. Schneider, G. Li, B. Sami, W. Shen, T. Berger, O. Diwald and J. Libuda, *Phys. Chem. Chem. Phys.*, 2018, **20**, 24858–24868.
- 14 G. Yi, Z. Xu, G. Guo, K. Tanaka and Y. Yuan, *Chem. Phys. Lett.*, 2009, **479**, 128–132.
- 15 Z.-A. Qiao, Z. Wu and S. Dai, *ChemSusChem*, 2013, **6**, 1821–1833.
- 16 C. Zhang, Y. Chen, H. Wang, Z. Li, K. Zheng, S. Li and G. Li, *Nano Res.*, 2018, **11**, 2139–2148.
- 17 N. Ta, J. Liu and W. Shen, *Chin. J. Catal.*, 2013, **34**, 838–850.
- 18 W. Li, C. Liu, H. Abroshan, Q. Ge, X. Yang, H. Xu and G. Li, *J. Phys. Chem. C*, 2016, **120**, 10261–10267.
- 19 J. Zhang, Z. Li, J. Huang, C. Liu, F. Hong, K. Zheng and G. Li, *Nanoscale*, 2017, **9**, 16879–16886.
- 20 R. Jin, C. Zeng, M. Zhou and Y. Chen, *Chem. Rev.*, 2016, **116**, 10346–10413.
- 21 Q. Yao, T. Chen, X. Yuan and J. Xie, *Acc. Chem. Res.*, 2018, **51**, 1338–1348.
- 22 G. Li and R. Jin, *Acc. Chem. Res.*, 2013, **46**, 1749–1758.
- 23 C. Liu, C. Yan, J. Lin, C. Yu, J. Huang and G. Li, *J. Mater. Chem. A*, 2015, **3**, 20167–20173.
- 24 C. Liu, H. Abroshan, C. Yan, G. Li and M. Haruta, *ACS Catal.*, 2016, **6**, 92–99.
- 25 Z. Li, C. Liu, H. Abroshan, D. R. Kauffman and G. Li, *ACS Catal.*, 2017, **7**, 3368–3374.
- 26 Z. Li, W. Li, H. Abroshan, Q. Ge, Y. Zhou, C. Zhang, G. Li and R. Jin, *Nanoscale*, 2018, **10**, 6558–6565.
- 27 S. Yang and L. Gao, *J. Am. Chem. Soc.*, 2006, **128**, 9330–9331.
- 28 J. Li, N. Ta, Y. Li and W. Shen, *Chin. J. Catal.*, 2008, **29**, 823–830.
- 29 H. X. Mai, L. D. Sun, Y. W. Zhang, R. Si, W. Feng, H. P. Zhang, H. C. Liu and C. H. Yan, *J. Phys. Chem. B*, 2005, **109**, 24380–24385.
- 30 J. Lin, W. Li, C. Liu, P. Huang, M. Zhu, Q. Ge and G. Li, *Nanoscale*, 2015, **7**, 13663–13670.
- 31 G. Li and R. Jin, *J. Am. Chem. Soc.*, 2014, **136**, 11347–11354.
- 32 R. Si and M. Flytzani-Stephanopoulos, *Angew. Chem., Int. Ed.*, 2008, **47**, 2884–2887.
- 33 O. F. Odio, L. Lartundo-Rojas, P. Santiago-Jacinto, R. Martínez and E. Reguera, *J. Phys. Chem. C*, 2014, **118**, 2776–2791.
- 34 N. Sutradhar, A. Sinhamahapatra and S. Pahari, *J. Phys. Chem. C*, 2011, **115**, 7628–7637.
- 35 S. Wei, X. Fu, W. Wang, Z. Jin, Q. Song and C. Jia, *J. Phys. Chem. C*, 2018, **122**, 4928–4936.
- 36 T. Venkov, K. Fajerwerg, L. Delannoy, H. Klimev, K. Hadjiivanov and C. Louis, *Appl. Catal., A*, 2006, **301**, 106–114.

